

# THE FIRST OBSERVATIONS OF LOW REDSHIFT DAMPED LYMAN- $\alpha$ SYSTEMS WITH THE COSMIC ORIGINS SPECTROGRAPH<sup>1</sup>

J.D. MEIRING<sup>2</sup>, T. M. TRIPP<sup>2</sup>, J. X. PROCHASKA<sup>3</sup>, J. TUMLINSON<sup>4</sup>, J. WERK<sup>3</sup>, E. B. JENKINS<sup>5</sup>, C. THOM<sup>4</sup>, J.M. O'MEARA<sup>6</sup>, K. R. SEMBACH<sup>4</sup>

*Draft version September 20, 2018*

## ABSTRACT

We report on the first Cosmic Origins Spectrograph (COS) observations of damped and sub-damped Lyman- $\alpha$  (DLA) systems discovered in a new survey of the gaseous halos of low-redshift galaxies. From observations of 37 sightlines, we have discovered three DLAs and four sub-DLAs. We measure the neutral gas density  $\Omega_{\text{H I}}$ , and redshift density  $dN/dz$ , of DLA and sub-DLA systems at  $z < 0.35$ . We find  $dN/dz=0.25^{+0.24}_{-0.14}$  and  $\Omega_{\text{H I}}=1.4^{+1.3}_{-0.7} \times 10^{-3}$  for DLAs, and  $dN/dz=0.08^{+0.19}_{-0.06}$  with  $\Omega_{\text{H I}}=4.2^{+9.6}_{-3.5} \times 10^{-5}$  for sub-DLAs over a redshift path  $\Delta z = 11.9$ . To demonstrate the scientific potential of such systems, we present a detailed analysis of the DLA at  $z_{\text{abs}}=0.1140$  in the spectrum of SDSS J1009+0713. Profile fits to the absorption lines determine  $\log N(\text{H I})=20.68 \pm 0.10$  with a metallicity determined from the undepleted element Sulfur of  $[\text{S}/\text{H}]=-0.62 \pm 0.18$ . The abundance pattern of this DLA is similar to that of higher  $z$  DLAs, showing mild depletion of the refractory elements Fe and Ti with  $[\text{S}/\text{Fe}]=+0.24 \pm 0.22$  and  $[\text{S}/\text{Ti}]=+0.28 \pm 0.15$ . Nitrogen is underabundant in this system with  $[\text{N}/\text{H}]=-1.40 \pm 0.14$ , placing this DLA below the plateau of the  $[\text{N}/\alpha]$  measurements in the local Universe at similar metallicities. This DLA has a simple kinematic structure with only two components required to fit the profiles and a kinematic width of  $\Delta v_{90}=52 \text{ km s}^{-1}$ . Imaging of the QSO field with HST/WFC3 reveals a spiral galaxy at very small impact parameter to the QSO and several galaxies within  $10''$ , or 20 comoving kpc at the redshift of the DLA. Followup spectra with LRIS on the Keck telescope reveal that none of the nearby galaxies are at the redshift of the DLA. The spiral galaxy is identified as the host galaxy of the QSO based on the near perfect alignment of the nucleus and disk of the galaxy as well as spectra of an H II region showing emission lines at the QSO redshift. A small feature appears  $0.70''$  from the nucleus of the QSO after PSF subtraction, providing another candidate for the host galaxy of the DLA system. Even with these supporting data, we are unable to unambiguously identify the host galaxy of the DLA, exemplifying some of the difficulties in determining DLA hosts even at low redshift.

*Subject headings:* none yet

## 1. INTRODUCTION

Quasar (QSO) absorption line systems provide a unique means to study the intergalactic medium, as well as the interstellar medium (ISM) of galaxies at all redshifts. Resonance absorption lines from metallic ions in the ISM of distant galaxies along the line of sight to a QSO provide a powerful method for the determination of chemical abundances at high redshifts, and also reveal the properties of low-density gas that is difficult or even impossible to detect with any other method, even in the nearby Universe. As this method is independent of the luminosity of the intervening galaxy, it is a relatively unbiased tracer of the chemical evolution of the Universe

as a whole.

The H I  $\lambda$  1215 absorption line in Damped Lyman- $\alpha$  systems (DLAs,  $\log N(\text{H I}) > 20.3$ ) and sub-DLAs ( $19.0 < \log N(\text{H I}) < 20.3$ ) can be fit for accurate column density measurements due to the extended damping wings in the profile. DLAs and sub-DLA systems have been shown to contain the majority of the neutral gas in the Universe (Wolfe et al. 1995; Péroux et al. 2003b; Prochaska, Herbert-Fort & Wolfe 2005; Noterdaeme et al. 2009).

The DLAs are of particular importance for galactic chemical evolution studies. With such high column densities, the absorption lines from metal atoms are easily visible. Also, systems with high column densities are expected to remain mainly neutral due to self shielding, alleviating the need for uncertain ionization corrections to the abundances.

There is still much debate as to the nature of the galaxies hosting DLAs and sub-DLAs. Even at low redshift, finding a faint galaxy near the bright point source of the QSO is challenging. At higher redshift, the cosmological dimming of surface brightness ( $\mu \propto (1+z)^4$ ) makes galaxy detections even more difficult. Nonetheless, these systems are a unique laboratory to study the ISM of galaxies over a wide range of redshifts.

At  $z > 1.65$ , the Lyman- $\alpha$  line shifts above the atmo-

<sup>1</sup> Based on observations made with the NASA/ESA Hubble Space Telescope, obtained at the Space Telescope Science Institute, which is operated by the Association of Universities for Research in Astronomy, Inc., under NASA contract NAS 5-26555. These observations are associated with program GO11598.

<sup>2</sup> Department of Astronomy, University of Massachusetts, Amherst, MA 01003, USA

<sup>3</sup> University of California Observatories-Lick Observatory, UC Santa Cruz, CA 95064, USA

<sup>4</sup> Space Telescope Science Institute, 3700 San Martin Drive, Baltimore, MD 21218, USA

<sup>5</sup> Princeton University Observatory, Princeton, NJ 08544, USA

<sup>6</sup> Department of Chemistry and Physics, St. Michaels College, One Winooski Park, Colchester, VT 05439, USA

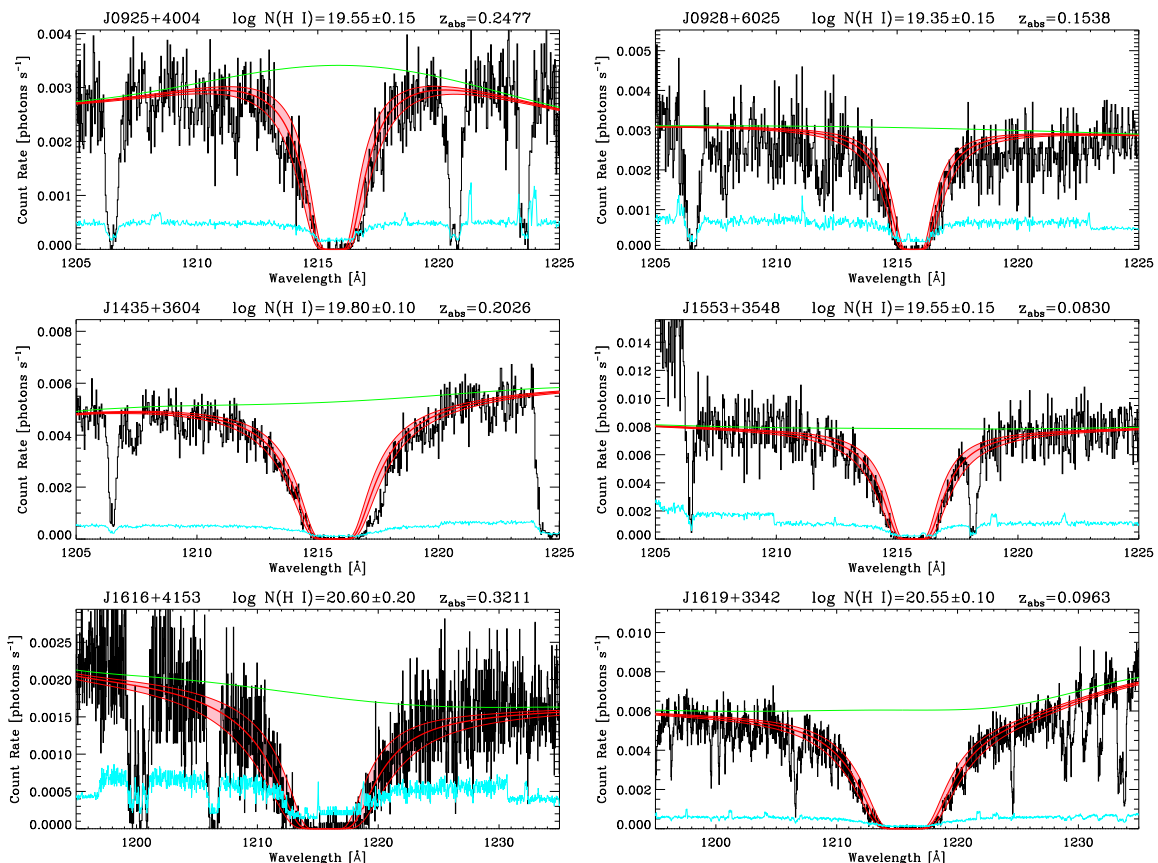


**Figure 1.** Lyman- $\alpha$  absorption lines from the DLAs and sub-DLAs in this sample. The solid green line is the adopted continuum, and the best fit profiles are bracketed by profiles with column densities  $1\sigma$  above and below the best fit value. The  $1\sigma$  flux uncertainty is shown in cyan below the data.

spheric cutoff at  $\sim 3000\text{\AA}$ , and ground based surveys can efficiently search for DLA systems. Several such surveys have determined the  $z > 2$  neutral gas density  $\Omega_{\text{H I}}$  (Wolfe et al. 1995; Storrie-Lombardi & Wolfe 2000; Prochaska, Herbert-Fort & Wolfe 2005; Noterdaeme et al. 2009). At lower redshifts, space-based spectra are necessary to measure the neutral hydrogen column densities in the UV. As DLAs (and QSOs that are bright enough in the far ultraviolet (FUV) to be accessible to previous UV spectrographs) are relatively rare, the number of such systems currently known at  $z < 1$  is small compared to available samples at high redshift.

The Cosmic Origins Spectrograph (COS) is a new instrument package (Froning & Green 2009) installed on the Hubble Space Telescope that enables us to study these absorbers at low redshift with unprecedented efficiency. As  $z < 0.5$  spans  $\sim 40$  percent of the age of the universe, the low redshift absorbers accessible with COS are crucial for understanding cosmic chemical evolution and the cosmological gas mass density and for linking their properties to their higher redshift counterparts.

In this paper, we report on the first DLA systems observed with COS. We present a detailed analysis of one such system, a DLA in the line of sight to the QSO SDSS J1009+0713, to illustrate the scientific potential of the observations. The structure of the paper is as follows. In §2 we describe in general the HST program and data reduction methods we have used for the COS spectra.

In §3 we describe the observations of the field of SDSS J1009+0713, including the ground based Keck/HIRES spectra of the QSO, the COS UV spectra, and imaging of the field with the Wide Field Camera 3 (WFC3). In §4 we derive chemical abundances for this system, discuss the physical state of the gas as determined by the CI and C II\* lines, and discuss the properties of the galaxies in the field as seen in the WFC3 images. In §5 we combine the measurements of  $N(\text{H I})$  from other absorbers in this program to measure the cosmological mass density of neutral gas,  $\Omega_{\text{H I}}$ , at  $z < 0.35$  in a blind survey with  $\Delta z \sim 12$ . Conclusions are summarized in §6. Throughout this paper, we adopt a cosmological model with  $\Omega_m = 0.30$ ,  $\Omega_\Lambda = 0.70$ , and  $H_0 = 70 \text{ km s}^{-1} \text{ Mpc}^{-1}$ .

## 2. PROGRAM SUMMARY AND OBSERVATIONS

The targets presented here were observed as part of program GO11598, a program focused on studying multiphase baryons in the halos of  $L \gtrsim L^*$  galaxies at 15-150 kpc impact parameters. Target QSOs for this program were selected based on sufficient FUV flux and the presence of a galaxy seen in the Sloan Digital Sky Survey (SDSS, York et al. 2000) with impact parameter  $\rho < 150$  kpc and a spectroscopic or photometric redshift  $0.15 < z < 0.35$ . Sightlines with strong Mg II systems seen in the SDSS spectra were avoided due to the possibility of a Lyman-limit system (LLS) at  $z \lesssim 0.35$  which would block the FUV flux. In total, 39 sightlines will ultimately be observed in this program. Followup ground-

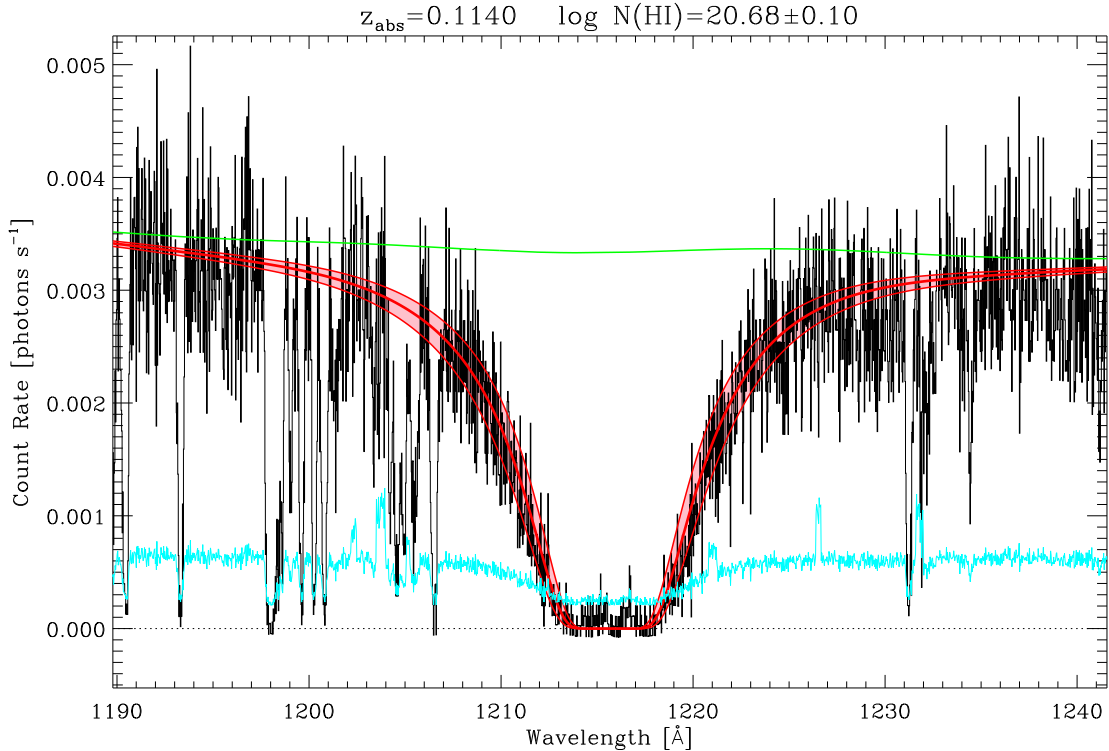


**Figure 2.** The fit to the DLA line in the spectrum of SDSS J1009+0713. The solid green line represents the adopted continuum and the red lines are the best fit model with  $\log N=20.68$  bracketed by profiles with column densities  $1\sigma=0.10$  dex above and below the best fit value. The  $1\sigma$  flux uncertainty is shown in cyan below the data.

based spectra with the Low Resolution Imaging Spectrometer (LRIS) on Keck will provide for redshifts, star formation rates and metallicities of the target galaxies as well as galaxies in the field.

These COS data were processed with CALCOS version 2.12 during retrieval from the archive. The individual reduced and wavelength calibrated x1d files were then coadded using custom software. In short, the gross source and background counts in each wavelength bin are summed after the bins are aligned in wavelength space by using a cross correlation analysis to allow for small shifts due to inaccuracies in the wavelength calibration provided by CALCOS. Simultaneously, an effective integration time at each wavelength bin is created which the total counts are ultimately divided by, returning the source count rate in photon  $s^{-1}$ . During coaddition, the spectra are background subtracted and also corrected for the fixed pattern noise caused by grid wires above the micro-channel plate detectors using a reference file provided by the COS instrument team. COS has extremely low backgrounds, and consequently, in some cases there are very few counts in the cores of strong absorption lines. We determine uncertainties directly from the accumulated counts, using Poisson statistics (see, e.g., Gehrels 1986) when the count numbers are low.

The spectra were binned by 3 pixels, as the raw COS data are oversampled with a  $\sim 6$  pixel wide resolution element. All subsequent measurements and analysis were performed on the binned spectra. The binned spectra have a resolution of  $\sim 15$   $\text{km s}^{-1}$  per resolution element. The S/N of these COS spectra range from 7 – 15 per resolution element.

The DLA and sub-DLA systems that we have discov-

ered in this program are shown in Figures 1 and 2. The Lyman alpha lines from the systems were fitted using a single component with the continuum and profile fit simultaneously. The redshifts of the systems were determined from the metal lines, which with narrow features provide for a more accurate redshift determination. In total, we find three DLA systems and four sub-DLA systems in these COS data. Absorption redshifts and neutral hydrogen column densities for the systems are given in Table 1. Errors on  $N_{\text{HI}}$  given in Table 1 have been estimated by eye and are dominated by the continuum placement uncertainty.

### 3. THE DLA IN SDSS J1009+0713

In order to illustrate the capabilities of COS for future observations of DLA systems, we present a detailed analysis of one system observed in the sample here. Similar analyses for the complete DLA and sub-DLA sample will be given in a forthcoming paper. SDSS J1009+0713 ( $\alpha=10:09:02.0$ ,  $\delta=+07:13:43.8$ ,  $z_{em} = 0.456$ ), is an optically bright ( $m_g=17.08$ ,  $M_g = -24.7$ ) QSO observed in the SDSS. This QSO was chosen for the survey of galaxy halos due to the presence of an  $L \sim L^*$  galaxy at an impact parameter of 60 kpc at redshift  $z = 0.228$ . The DLA described here was serendipitously discovered in the COS spectrum of the QSO. No absorption lines from this system are present in the SDSS spectrum of the QSO, as the Mg II  $\lambda\lambda$  2798, 2802 lines which are typically strong enough to be seen in the SDSS spectra fall at 3115-3125 Å and are below the wavelength range that the SDSS spectra cover. In this section, we present a detailed analysis of this system, including the COS and Keck High Resolution Spectrometer (HIRES) spectra as

well as followup imaging with the Wide Field Camera 3 (WFC3).

### 3.1. COS Spectra

These COS data were acquired on 29-30 March 2010 in three orbits as Visit 13 in program GO11598. Two exposures were obtained with the G130M grating at central wavelengths of 1291 and 1309 Å with exposure times of 1497 and 2191 s. Similarly, two exposures were taken with the G160M grating at central wavelengths of 1577 and 1600 Å with exposure times of 2002 and 2007 s.

The DLA line of this system was fit with a single component centered at  $z_{abs}=0.1140$  with a best solution of  $\log N(\text{H I})=20.68\pm 0.10$ . The fit to the DLA line is shown in Figure 2. Profiles with column densities  $1\sigma$  above and below the best fit value are also shown in Figure 2.

Absorption lines from multiple species are shown in the left panel of Figure 6. We detect lines from N I  $\lambda\lambda$  1134, 1199, 1200, 1201; O I  $\lambda$  1302; Si II  $\lambda\lambda$  1190, 1304, 1526; S II  $\lambda\lambda$  1250, 1253, 1259; Fe II  $\lambda\lambda$  1142, 1143, 1144; Ni II  $\lambda$  1317. A Lyman limit system (LLS) at  $z_{abs}=0.3556$  blocks the continuum blueward of  $\sim 1240$  Å (see Tumlinson et al. (2010) for an analysis of the LLS) or  $\sim 1115$  Å in the rest frame of the DLA.

There are only two H<sub>2</sub> lines covered in the COS spectrum due to the presence of the LLS. The Lyman band ( $X^1\Sigma_g^+ - B^1\Sigma_u^+$ ) transitions from the (1-0) band which have rest frame wavelengths  $\lambda < 1109$  Å are all blocked by the LLS. Only the H<sub>2</sub>  $\lambda\lambda$  1120, 1125 lines resulting from the (0-0) transitions are covered in the COS data. These lines are however blended with strong high Lyman series absorption lines from the LLS; consequently no direct indicator of molecular gas exists for this DLA.

The COS spectra cover the lines of C IV  $\lambda\lambda$  1548, 1550 as well as the Si IV  $\lambda\lambda$  1393, 1402 transitions. The C IV lines lie at the edge of the detector where the sensitivity is low and only the C IV  $\lambda$  1548 line is minimally detected at S/N $\sim$ 3. The Si IV  $\lambda$  1393 line is blended with the Lyman- $\alpha$  absorption line from a  $z_{abs}=0.2774$  system, and there is no detection of the Si IV  $\lambda$  1402 with S/N $\sim$ 5 in the region.

### 3.2. Keck-HIRES Spectra

Optical spectra of SDSS J1009+0713 were obtained with the Keck-II/HIRES spectrograph (Vogt et al. 1994) on the night of 26 March 2010. The S/N of the data ranges from  $\lesssim 5$  per  $1.8 \text{ km s}^{-1}$  pixel at 3200 Å to  $\sim 20$  at 4500 Å. These data provide coverage from 2750-4000 Å in the rest frame of the  $z_{abs}=0.1140$  DLA, and hence include the lines of Mg II  $\lambda\lambda$  2796, 2803, Mg I  $\lambda$  2852, Ti II  $\lambda\lambda$  3242, 3384, and Ca II  $\lambda\lambda$  3934, 3969. The Mg I  $\lambda$  2852 line is partially blended with the Fe II  $\lambda$  2344 line from the  $z_{abs}=0.3558$  LLS, as can be seen in Figure 6. In addition, with higher resolution (R=44,000) than the COS spectra (R $\sim$ 20,000), these data provide valuable constraints on the kinematics and doppler parameters of the lines that are blended at the resolution of COS.

These data were processed with the Keck/HIRES reduction code HIRESREDUX in IDL<sup>7</sup>. The right panel of Figure 6 shows the HIRES spectra of several near-UV

<sup>7</sup> Available at <http://www.ucolick.org/~xavier/HIREDUX/>

**Table 1**

Properties of the  $z_{abs} < 0.35$  DLAs and sub-DLAs in this survey.

QSO	$z_{em}$	$z_{abs}$	$\log N(\text{H I})$ $\text{cm}^{-2}$
SDSS J092554.70+400414.1	0.471	0.2477	19.55 $\pm$ 0.15
SDSS J092837.98+602521.0	0.295	0.1538	19.35 $\pm$ 0.15
SDSS J100902.06+071343.8	0.456	0.1140	20.68 $\pm$ 0.10
SDSS J143511.53+360437.2	0.429	0.2026	19.80 $\pm$ 0.10
SDSS J155304.92+354828.6	0.722	0.0830	19.55 $\pm$ 0.15
SDSS J161649.42+415416.3	0.440	0.3211	20.60 $\pm$ 0.20
SDSS J161916.54+334238.4	0.471	0.0963	20.55 $\pm$ 0.10

**Table 2**

AB magnitudes and position offsets for the galaxies near SDSS J1009+0713. Identifiers are based on the position angle and distance from the target QSO.

ID	$\Delta\alpha$ "	$\Delta\delta$ "	$m_{625W}$ AB	$m_{390W}$ AB	$z_{gal}$
170_9	+1.58	-9.27	21.33 $\pm$ 0.08	22.16 $\pm$ 0.12	0.35569
86_4	+2.87	+0.16	23.21 $\pm$ 0.21	24.10 $\pm$ 0.20	0.35455
80_5	+4.00	+0.81	22.50 $\pm$ 0.12	23.09 $\pm$ 0.18	0.87899
92_7	+6.26	-0.44	23.67 $\pm$ 0.37	24.45 $\pm$ 0.36	1.283?

(NUV) and optical absorption lines that were observed in this DLA.

The profile was fit with only two components having doppler widths of  $b_{eff} = 10.6$  and  $12.9 \text{ km s}^{-1}$  and centroid velocities of  $-6.6$  and  $+21.5 \text{ km s}^{-1}$  respectively. The majority of the low ionization gas appears to be in the  $v = -6.6 \text{ km s}^{-1}$  component, as this component is strongest in all of the non-saturated absorption lines detected here.

### 3.3. WFC3 Imaging and Keck LRIS Spectra

The SDSS images show no obvious candidates for the  $z_{abs}=0.1140$  DLA. In order to determine the nature of the host galaxy of the DLA system, we acquired imaging in the F390W and F625W filters of this field using the Wide Field Camera 3 (WFC3) onboard the HST. Six exposures were taken in both filters in a dither pattern to eliminate the effects of bad pixels and cosmic rays. Total exposure time was 2370 and 2256 seconds in the F390W and F625W filters respectively.

Even with the superb image quality and resolution that WFC3 enables, galaxies at small impact parameter to the central bright QSO may only appear after subtracting the QSO with a suitably chosen Point Spread Function (PSF). The PSFs used here were acquired from the Tiny Tim online interface<sup>8</sup> at the pixel coordinates appropriate for the position of the QSO in the images. This PSF was then interactively subtracted from each individual dithered image with IDP3<sup>9</sup> and the subtracted images were then drizzle combined with MULTIDRIZZLE. The final drizzled images are shown in Figure 3. A color combined image was also created from the PSF subtracted images, and is shown in Figure 4. The F625W, F390W, and an average of the two were used in the red, blue, and green channels of the color image and the images were scaled using the *asinh* scaling described in Lupton et al. (2004).

<sup>8</sup> Available at <http://www.stecf.org/instruments/TinyTim/tinytimweb>

<sup>9</sup> Available at <http://mips.as.arizona.edu/MIPS/IDP3/>

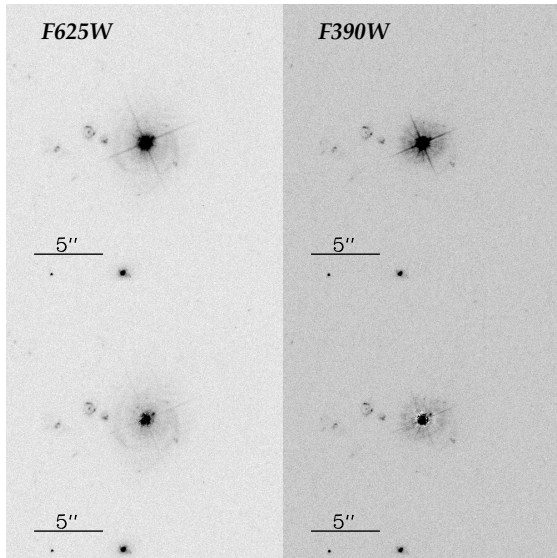


**Figure 3.** F625 and F390W band images of the field of SDSS J1009+0713. The PSF subtracted images are shown in the bottom row.

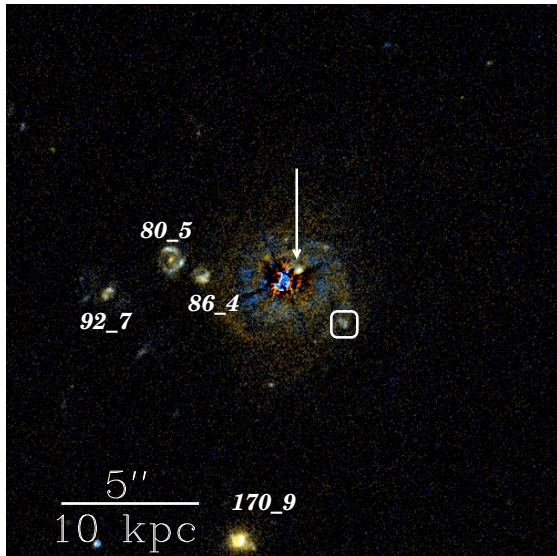


**Figure 4.** Color combined PSF subtracted images of the field of J1009+0713 in the F625W and F390W filters. The red channel is the F625W band image, the blue channel is the F390W band image, and the green channel is an average of the two. 5 arcseconds is  $\sim 10$  kpc at  $z = 0.114$ . The arrow marks the location of the small feature visible after PSF subtraction. An H II region is marked with a box southwest of the center of the galaxy. North is up and east is to the left.

Multiple galaxies are seen in these WFC3 images within  $10''$  of the QSO, or  $\sim 20$  kpc at  $z = 0.1140$ . A large spiral galaxy is clearly seen in Figures 3 and 4. Spectra of objects 80\_5, 86\_4, 92\_7 and 170\_9 as well as the H II region labelled in Figure 4 were obtained with Keck/LRIS<sup>10</sup>. A  $1''$  slit was used and aligned such that multiple galaxies and the H II region marked in Figure 4 were observed simultaneously. Emission lines from O III]  $\lambda\lambda$  4960,5008 and H  $\beta$   $\lambda$  4862 are

<sup>10</sup> Labels for galaxies in the field are based on the position angle and distance from the QSO; i.e. galaxy 80\_5 is at a position angle of 80 degrees east of north and 5 arcseconds from the center of the QSO.

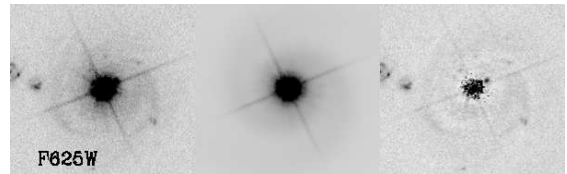


**Figure 5.** Left - The WFC3 image of the QSO. Center - The model adopted from GALFIT. Right - The residual image. Some emission is left over in the point source in due to saturation effects. All frames have identical scaling.

clearly seen in galaxies 86\_4 and 170\_9 placing them at  $z = 0.35458$  and  $z = 0.35557$  respectively. These two galaxies are likely associated with a LLS at  $z_{abs}=0.3556$  (see Tumlinson et al. (2010) for an analysis of the LLS).

Two emission features from galaxy 80\_5 are seen at 7004 and 8158  $\text{\AA}$ , which we interpret as O II]  $\lambda$  3727 and H  $\gamma$  4341 at  $z = 0.87899$ . A single strong emission line at 8508  $\text{\AA}$  is observed in the spectrum of galaxy 92\_7. No prominent emission lines expected from a galaxy at a redshift  $z = 0.1140$  correspond to this observed wavelength. Assuming this emission line is from O II]  $\lambda\lambda$  3727,3729 places this galaxy at  $z = 1.283$ .

Narrow emission lines from H  $\beta$   $\lambda$  4862 and O III]  $\lambda\lambda$  4960,5008 from the H II region in the spiral galaxy labelled in Figure 4 give a redshift of  $z = 0.45699$ . Some flux from the nucleus of the QSO is observed in the spectra, however no emission lines from another redshift were seen in the spectra increasing our confidence in the determination of the redshift of the H II region. Combined with the close alignment of the nucleus of the QSO and disk of the galaxy, we interpret the spiral galaxy to be the host of the QSO itself.

Emission lines from intervening galaxies are sometimes seen superimposed on the continuum of the QSO in SDSS spectra (Noterdaeme, Srianand & Mohan 2010; Borthakur et al. 2010), although most QSOs do not show such emission features in their spectrum even when strong absorption lines are seen. No narrow emission lines are seen in the SDSS spectrum of this QSO at the absorption redshift of the DLA or any other redshift.

## 4. RESULTS

### 4.1. Imaging

We performed aperture photometry on the galaxies in Figure 4 with APPHOT in IRAF. AB magnitudes are given in Table 2. Magnitudes have been corrected for Galactic dust extinction<sup>11</sup> from Schlegel, Finkbeiner & Davis (1998). As galaxies 170\_9, 80\_5, and 92\_7 are spectroscopically confirmed to be at significantly higher redshift than the absorption redshift of the DLA, an obvious question arises; where is the host galaxy of the DLA?

We have used the GALFIT software package (Peng et al. 2010) to fit a multicomponent profile to the F625W image of the QSO. A PSF for the nucleus, Sersic profile for the bulge, and exponential disk for the spiral structure was used in the fit. The best fit solution from GALFIT using these components gives  $m_B = 18.68$ ,  $m_D = 18.71$ , and  $m_N = 17.99$  where  $m_B$ ,  $m_D$  and  $m_N$  are the magnitudes of the bulge, disk and nucleus respectively. The combined magnitude of the bulge and disk

<sup>11</sup> The online version of the calculator is available at <http://nedwww.ipac.caltech.edu/forms/calculator.html>

is  $m_{tot} = 17.91$ , comparable to that of the nucleus. We show the results of the GALFIT decomposition in Figure 5.

The host galaxies of QSOs are known to be luminous, with  $L > L^*$ , and come from a variety of morphological types across the entire Hubble sequence (Bahcall et al. 1997; Hamilton, Casertano & Turnshek 2002). Given a measured apparent magnitude  $m_\lambda$ , the absolute magnitude  $M_\lambda$  is given by

$$M_\lambda = m_\lambda - 5 \log \left( \frac{D_L}{10 \text{ pc}} \right) - K_\lambda - A_\lambda \quad (1)$$

where  $D_L$  is the luminosity distance,  $K_\lambda$  is the k-correction and  $A_\lambda$  is the extinction due to the Galaxy. Based on the morphology of the galaxy seen in Figure 4, we assume a Sb type spectrum and find a K correction of  $K_\lambda = 0.25$  magnitudes in the F625W filter at  $z_{em} = 0.456$  and apply an extinction of  $A_\lambda = 0.05$  magnitudes giving  $M_{F625W} = -24.4$ . The median luminosity of radio loud QSO host galaxies in the sample of Hamilton, Casertano & Turnshek (2002) is  $M_V = -23.5$ , although galaxies classified as having spiral morphologies were typically more luminous than elliptical counterparts.

A small feature at small impact parameter appears more clearly in the PSF subtracted images shown in Figure 3 and is marked with an arrow in Figure 4. The angular separation from the nucleus of the QSO is 0.7 arcseconds, or  $\sim 1.5$  kpc at  $z = 0.114$ . It is possible that this is the host galaxy of the DLA, or perhaps an H II region in the QSO host galaxy. For example, if either of the galaxies labelled 80\_5 or 86\_4 in Figure 4 were placed at small impact parameter to the QSO, it would be difficult to disentangle the two even with the resolution of WFC3. The WFC3 grism is likely the best (if not only) way to definitively determine the redshift the spiral galaxy and object at small impact parameter seen in Figure 4.

This QSO does show radio continuum emission, with a central source and two lobes detected in the FIRST survey with peak emission of  $\sim 6$  mJy (Becker, White & Helfand 1995). Radio loud QSOs are almost all found in elliptical galaxies; out of the 26 radio loud QSOs observed by Hamilton, Casertano & Turnshek (2002), only 4 had spiral type morphologies (16 percent).

#### 4.2. Column Densities and Abundances

Logarithmic abundances (defined as  $[X/H] = \log X - \log H - [X/H]_\odot$ ) for the DLA system as determined by the profile fits to the COS and HIRES data are presented here. Solar system reference abundances ( $[X/H]_\odot$ ) are taken from Lodders (2003). Rest frame wavelengths as well as  $f$  values are taken from Morton (2003) for all lines aside from the C I lines, for which we use the revised  $f$  values determined in Jenkins & Tripp (2001) and Ni II  $\lambda\lambda$  1317, 1370 lines for which we use the revised  $f$  values from Jenkins & Tripp (2006).

The COS spectra were fit using the component structure determined with the higher resolution ground based Keck spectra. Both the doppler parameters and velocity centroids were held fixed in the fits, and multiple transitions were fit simultaneously where possible (i.e. the S II  $\lambda\lambda$  1250, 1253, 1259 lines were all fit simultane-

ously). The synthetic Voigt profiles were convolved with the COS line spread functions (LSF)<sup>12</sup> as determined by the COS science team at the nearest tabulated wavelength (Ghavamian et al. 2009). The Keck/HIRES spectra were convolved with a gaussian line spread function with FWHM=2.5 pixels. Profile fitting was performed using the profile fit code of Fitzpatrick & Spitzer (1994).

In the case of a particular resonance line not being detected in these data, we have used the following procedure to determine a limiting column density for the line. 1) First, we again use the doppler parameters and velocity centroids as determined in the higher resolution data. 2) We take the column densities for one of the better constrained fits to determine the ratio of the column densities in each of the components. 3) Synthetic Voigt profiles are then produced and multiplied by the normalized flux and an equivalent width is determined. The integration and statistics are performed over a region from the lowest to highest velocity component, with an additional 30 km s<sup>-1</sup> (or  $\sim 2$  resolution elements) on each end to ensure that all of the absorption is taken into account. 4) The significance of the line is determined by calculating  $EW/\sigma_{tot}$  where  $\sigma_{tot} = \sqrt{\sigma_c^2 + \sigma_p^2}$  and  $\sigma_c$  is the uncertainty in the EW due to the continuum placement and  $\sigma_p$  is the uncertainty. This again perhaps indicates that the spiral seen in Figure 4 is not the host of the DLA galaxy. due to photon noise. 5) The column densities are then increased until the line has a 3 $\sigma$  significance.

Strong transitions such as O I  $\lambda$  1302, C II  $\lambda$  1334 and Mg II  $\lambda\lambda$  2793, 2803 are almost universally saturated, and only lower limits to the column densities can be determined by fits to these lines. Lower limits in these cases were determined by creating synthetic Voigt profiles and increasing the column densities in the components until the profile reached the observed flux at the line core. We have determined a permissible range of  $15.35 < N(\text{Mg II}) < 16.0$  which is equivalent to  $-0.9 < [\text{Mg}/\text{H}] < -0.2$  by measuring an upper limit on the weak transition of Mg II  $\lambda$  1239.

As the component structure in the more highly ionized gas traced by the C IV  $\lambda\lambda$  1548, 1550 and Si IV  $\lambda\lambda$  1393, 1402 lines is often different than that of the low ions and the S/N in the region of the C IV lines is too low to discern the component structure, we have measured the column density of C IV by direct integration of the line using the apparent optical depth (AOD) method. We determine  $\log N(\text{C IV}) = 13.86 \pm 0.20$ . We also place an upper limit on the column density of Si IV based on the non detection of the Si IV  $\lambda$  1402 line of  $\log N(\text{Si IV}) < 13.3$ .

The depletion in this system is mild with  $[\text{S}/\text{Fe}] = +0.24 \pm 0.22$ ,  $[\text{S}/\text{Ti}] = +0.28 \pm 0.15$  and  $[\text{S}/\text{Ni}] = +0.35 \pm 0.22$ , even less than what is seen in the halo of the Milky Way (Welty et al. 1997). Depletion levels in the ISM of the Milky Way are seen to vary over two orders of magnitude, from  $[\text{Zn}/\text{Fe}] > +2$  in cold clouds to  $[\text{Zn}/\text{Fe}] \sim +0.5$  in the halo of the Milky Way (Savage & Sembach 1996; Jenkins 2009). We note however that similar mild depletion was seen

<sup>12</sup> Tabulated LSFs for COS are available at [http://www.stsci.edu/hst/cos/performance/spectral\\_resolution/](http://www.stsci.edu/hst/cos/performance/spectral_resolution/)

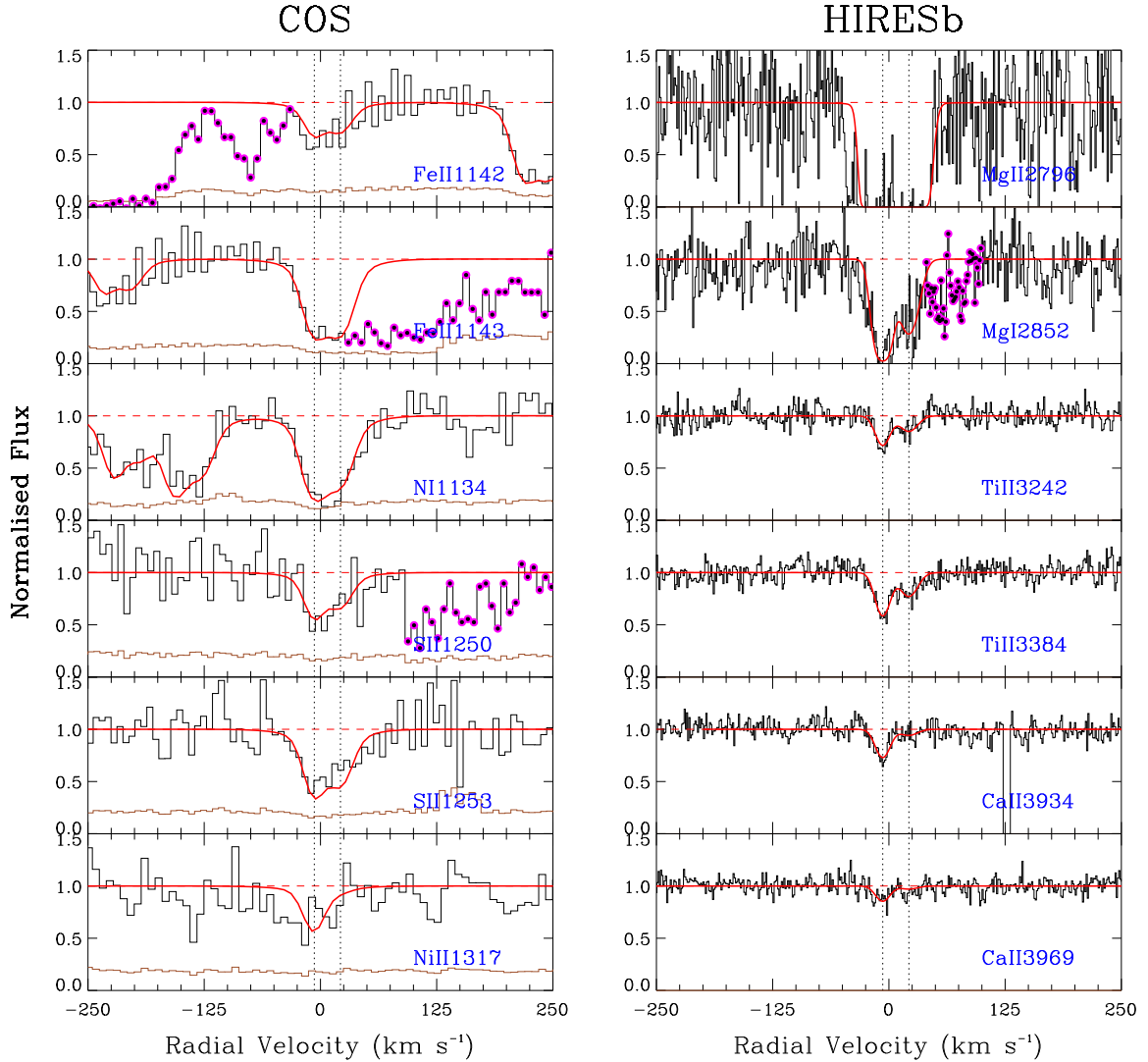


**Figure 6.** Velocity plots for several lines detected in the COS and HIRES spectra towards SDSS J1009+0713 at  $z_{abs}=0.1140$ . The theoretical best fit profile is shown in red, and the  $1\sigma$  error in the COS spectra is shown below the data in cyan. The dashed vertical lines denote the positions of the centroids of the components used in the fits. Unrelated interloping features from other systems are marked with magenta circles. Profile fits to nearby members in the multiplets are shown in the N I  $\lambda$  1134 and Fe II  $\lambda$  1142 lines.

at very small impact parameter towards HS1543+593 (Bowen et al. 2005), a case in which the connection between the absorber and host galaxy is unambiguous.

We have used the model of the depletion patterns in the ISM of the Milky Way from Jenkins (2009) to analyze the depletion in this DLA system. In this model a single value ( $F_*$ ) indicates the overall level of depletion in a sightline, with larger values of  $F_*$  indicating higher levels of dust depletion. We find that the line of sight depletion factor  $F_* = -0.48 \pm 0.24$  for this DLA, implying an intrinsic metallicity of  $[Z/H] = -0.77 \pm 0.44$ , consistent with the metallicity determined from the S II lines. Such negative values of  $F_*$  are typically seen along sightlines with extremely low average densities in the halo of our Galaxy (Jenkins 2009) implying that the sightline passes through the outer edge of a dwarf galaxy.

Kinematically, the component structure of this DLA is extremely simple (see Figure 6). Only two components

**Table 3**  
Total column densities and abundances for the dominant ions in the  $z_{abs}=0.1140$  DLA system.

Element	$\log N(X)$	$[X/H]$
H	$20.68 \pm 0.10$	
C	$>15.90$	$> -1.2$
N	$15.11 \pm 0.10$	$-1.40 \pm 0.14$
O	$>16.00$	$> -1.40$
Mg	$>15.35, <16.0$	$> -0.9, < -0.2$
Si	$>15.00$	$> -1.2$
P	$<13.80$	$< -0.34$
S	$15.25 \pm 0.12$	$-0.62 \pm 0.16$
Ti	$12.70 \pm 0.03$	$-0.90 \pm 0.10$
Fe	$15.29 \pm 0.17$	$-0.86 \pm 0.20$
Ni	$13.93 \pm 0.18$	$-0.97 \pm 0.20$

are required to fit the profiles of the absorption lines. The kinematic width  $\Delta v_{90}$  (defined as the region where 90

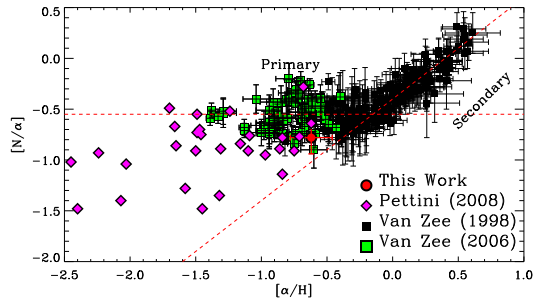


**Figure 7.**  $[N/\alpha]$  vs.  $[\alpha/H]$  for this system (red point), high  $z$  DLAs from Pettini et al. (2008), H II regions in nearby dwarf galaxies from Van Zee & Haynes (2006), and H II regions in nearby massive spirals from Van Zee et al. (1998). The dotted lines denote the solar abundance.

percent of the apparent optical depth in the line occurs) has often been used as an indicator of the kinematics of QSO absorption line systems (Prochaska & Wolfe 1997; Ledoux et al. 2006). We find a kinematic width for this system of  $\Delta v_{90} = 52 \text{ km s}^{-1}$  based on the Ti II  $\lambda 3384$  line.

#### 4.3. Nitrogen

The nucleosynthetic origins of N seem to include both primary (production of N from newly synthesized C via the CNO cycle) and secondary production (N produced again in the CNO cycle, but from previously created C and O from previous star formation) processes in intermediate mass stars (Marigo 2001). Of the  $\sim 30$  determinations of N abundances in DLA systems, all are at high  $z$  where the N I lines are redshifted into wavelengths accessible with ground based telescopes (Pettini et al. 2008; Henry & Prochaska 2007). Some constraints have been placed on nitrogen in low- $z$  sub-DLAs where, like the high- $z$  DLAs, Nitrogen is found to be underabundant (e.g., Tripp et al. (2005)).

Abundances from N can be readily obtained from optical spectra of H II regions in nearby star forming galaxies of a range of luminosities. The low luminosity galaxies from Van Zee & Haynes (2006) show a flat plateau in the  $[N/O]$  ratio with respect to metallicity, while the higher metallicity H II regions in Van Zee et al. (1998) show a sharp increase in  $[N/O]$  with increasing metallicity, indicative of secondary production of N.

Observations of N in extremely low metallicity DLAs are important for the study of N production and galactic chemical evolution in general (Pettini et al. 2008; Centurión et al. 2003). It is still yet to be seen if the  $[N/O]$  ratio in DLAs displays the same upturn as metallicity increases as most DLAs are metal poor and at high  $z$  the N I lines are often blended with the Lyman- $\alpha$  forest. The DLA presented here is the highest metallicity DLA with both N and  $\alpha$  abundance measurements.

In Figure 7 we show  $[N/\alpha]$  vs  $[\alpha/H]$  for H II regions in nearby galaxies from Van Zee et al. (1998); Van Zee & Haynes (2006), as well as the DLA sample from Pettini et al. (2008) and this DLA. The DLA from this work is shown with the red circular point, and lies below the “knee” of the diagram where N production transitions from primary to secondary production. The mean  $[N/\alpha]$  ratio from the samples of Van Zee et al. (1998) and (Van Zee & Haynes 2006) with  $[\alpha/H] < -0.3$

is  $\langle [N/\alpha] \rangle = -0.55 \pm 0.15$ ,  $3\sigma$  higher than seen in this DLA of  $[N/S] = -0.78 \pm 0.16$ . Pettini et al. (2008) note this discrepancy in the sample of DLAs shown in Figure 7 and propose that the lower values seen in high  $z$  DLAs could be due to the delayed enrichment of N with respect to O as the delay of  $\sim 250$  Myr is a greater fraction of the time available for star formation at high redshift than in local galaxies, so at high  $z$  this effect should be more pronounced. However, in this low- $z$  DLA we see the same decrement in  $[N/\alpha]$  compared to the values from local H II regions. It would be interesting to see if other high metallicity DLAs are also below the plateau, perhaps indicating a systematic offset in abundances determined via absorption and emission line diagnostics.

#### 4.4. C I and C II\*

Both C I and C II\* are important diagnostic resonance lines in the study of the ISM. Emission from the  $158 \mu\text{m}$  emission line of singly ionized carbon in the ISM of the Milky Way is the dominant coolant, and is expected to also be so in high- $z$  DLAs as well. This line originates from the transition between the  $^2P_{3/2}$  and  $^2P_{1/2}$  levels in the ground state of  $C^+$ . In the cold neutral medium (CNM,  $T \sim 10^2\text{K}$ ) the excited state is populated largely by collisions with hydrogen atoms, where in the more diffuse warm neutral medium (WNM,  $T \sim 10^4\text{K}$ ) both collisions with free electrons as well as photon pumping can populate the excited state (Wolfe, Prochaska & Gawiser 2003; Bowen et al. 2005).

In the WNM the electron density can be determined from observations of the C II and C II\* lines as

$$n(e) = 18.3 \sqrt{T_4} e^{0.091/T_4} \left[ \frac{N(\text{CII}^*)}{N(\text{CII})} \right] \text{ cm}^{-3} \quad (2)$$

where  $T_4$  is  $T/10^4\text{K}$  (Lehner, Wakker & Savage 2004). In the ISM of the Galaxy, the CNM is characterized by having large depletions of the refractory elements such as Fe and Ti relative to the volatile elements of S and Zn which do not condense onto dust grains. As the depletions levels in this DLA are modest, with  $[Ti/S] = -0.37 \pm 0.12$ , we assume that the sightline is passing through mainly a WNM. Depletion levels seen in the CNM of the Milky Way are typically ten times higher than what is observed in this DLA (Savage & Sembach 1996; Jenkins 2009).

The C II\*  $\lambda 1335$  line was not detected in these data, with  $S/N \sim 11$  per resolution element in the region around the line. We have used the procedure discussed above to determine a limiting column density of  $\log N(\text{C II}^*) < 13.7$ . We show a synthetic Voigt profile with this total column density overplotted on the data in Figure 8.

As was mentioned above the C II  $\lambda 1334$  is strongly saturated and only a limiting column density of  $\log N(\text{C II}) > 15.90$  can be determined from this transition. However, in sightlines with low depletion such as this Carbon is mildly depleted and we can use the S abundance to estimate a total C II column density assuming  $[C/S] \sim 0.0$ . The above analysis yields  $\log N(\text{C II}) = 16.45$ . Using the above values in Equation 2 with a temperature of 6000 K characteristic of the WNM the electron density is determined to be  $n(e) < 0.08 \text{ cm}^{-3}$ .

The cooling rate per H atom due to C II  $\lambda 158 \mu\text{m}$



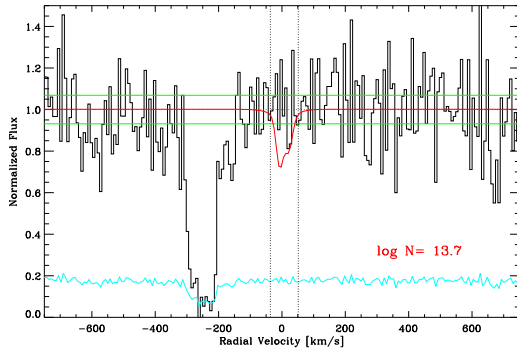


**Figure 8.** Synthetic Voigt profiles of the C II\*  $\lambda\lambda$  1335.6, 1335.7 lines overplotted on the COS data. We estimate the limiting column density of C II\* to be  $\log N(\text{C II}^*) \sim 13.70$ .

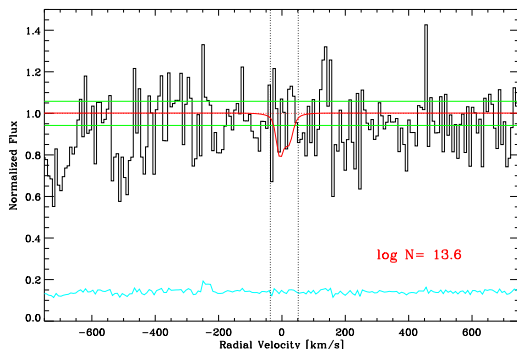


**Figure 9.** Synthetic Voigt profiles of the C I  $\lambda$  1277 line overplotted on the COS data. We estimate the limiting column density of C II\* to be  $\log N(\text{C II}^*) \sim 13.6$ .

emission can be estimated by

$$I_c = 2.89 \times 10^{-20} \left[ \frac{N(\text{C II}^*)}{N(\text{H I})} \right] \text{erg s}^{-1} (\text{H atom})^{-1} \quad (3)$$

(Lehner, Wakker & Savage 2004). Using the values above, we determine  $\log I_c < -26.5$ . This is typical of what has been observed in higher- $z$  DLA systems (Wolfe, Prochaska & Gawiser 2003; Lehner, Wakker & Savage 2004).

C I is a tracer of cold gas in the ISM, and is usually seen in DLA absorbers bearing  $\text{H}_2$  (Srianand et al. 2005). As such, C I absorption lines are indicative of cold, dense material in DLAs. The C I  $\lambda$  1277 line provides the strongest constraint on the  $\text{C}^0$  column density in the COS spectrum as the S/N in the region around the stronger transition of C I  $\lambda$  1560 was much lower. This line was not detected in the spectrum and we have determined a limiting column density of  $\log N(\text{C I}) < 13.6$  using the prescription above. In the two phase ISM model of Liszt (2002), the ratio of  $N(\text{C II})/N(\text{C I})$  is indicative of the gas density. The observed ratio of  $N(\text{C II})/N(\text{C I}) > 700$  in this system implies that  $n(\text{H}) < 10 \text{ cm}^{-3}$ .

## 5. THE COSMOLOGICAL NEUTRAL GAS MASS DENSITY

The sample of QSO sightlines from this HST program provides an opportunity to determine the incidence of DLA systems at low  $z$ , where there is a paucity of data due to the necessity of space-based observations. Ideally, a totally “blind” survey in which there is no prior information about the sightlines prior to observation provides

for the least amount of systematic biases in the determination of cosmological gas mass density.

In order to eliminate as much observational bias as possible, we have defined the redshift interval over which to search for DLAs and sub-DLAs with the following criteria. As these sightlines were selected due to the presence of a galaxy within impact parameters of  $\rho < 150 \text{ kpc}$ , we have excluded  $\pm 1000 \text{ km s}^{-1}$  around the redshift of the target galaxy in the search path to avoid biasing the sample artificially high due to the possible clustering of galaxies. At  $z \gtrsim 0.34$  the Mg II  $\lambda\lambda$  2796, 2803 lines are redshifted into the wavelength coverage of the SDSS. This program intentionally excluded sightlines with Mg II absorbers at  $z > 0.34$  due to the possibility of a LLS which would block the FUV flux, which in effect biases the sample against DLA detection at  $z > 0.34$ . To avoid this bias, we focus only on  $z < 0.34$ . In the cases where the emission redshift of the QSO is less than 0.34, we have excluded a  $3000 \text{ km s}^{-1}$  region blueward of the emission redshift.

The sub-DLAs towards SDSS J0925+4004, SDSS J0928+6025, and SDSS J1435+3604 have been excluded from the calculation as the absorption redshifts are within  $1000 \text{ km s}^{-1}$  of the redshift of the target galaxy, leaving 3 DLAs and 1 sub-DLA in the final sample. The total path length for the 37 sightlines in this sample using the definition above is  $\Delta z = 11.94$ , giving  $dN/dz = 0.25^{+0.24}_{-0.14}$  and  $dN/dz = 0.08^{+0.19}_{-0.06}$  for DLAs and sub-DLAs respectively, and assuming Poisson statistical errors from Gehrels (1986). The redshift density determined here is larger than the value determined in Rao, Turnshek & Nestor (2006) of  $dN/dz = 0.079 \pm 0.019$ , however the large statistical errors of this work make this difference unlikely to be statistically significant. From a large number of archived HST spectra, Ribaudo, Lehner & Howk (2010) find  $dN/dz = 0.37 \pm 0.10$  for all absorbers with  $N(\text{H I}) \gtrsim 17.0$ . The central value determined here for DLAs alone is  $\sim 2/3$  of the total redshift density of all optically thick systems, again suggesting that the redshift density of DLAs is lower than what is determined here.

The comoving gas mass density can be determined as

$$\Omega_{\text{H I}} = \frac{\mu m_{\text{H}} H_0 \Sigma N_{\text{H I}}}{\rho_c \Delta X} \quad (4)$$

where  $\mu = 1.3$  is the mean molecular mass of the gas taking into account the contribution of He,  $\rho_c$  is the critical density of the Universe,  $H_0$  is the Hubble constant, and  $m_{\text{H}}$  is the mass of the hydrogen atom (Wolfe, Gawiser & Prochaska 2005). The absorption distance  $dX$  is defined as

$$\frac{dX}{dz} = \frac{(1+z)^2}{\sqrt{\Omega_m(1+z)^3 + \Omega_k(1+z)^2 + \Omega_\Lambda}} \quad (5)$$

and is summed over each sightline in the sample. The total path length for the 37 QSOs in this sample using the criteria above is  $\Delta X = 15.1$ .

We find  $\Omega_{\text{H I}} = 1.4^{+1.3}_{-0.7} \times 10^{-3}$  and  $\Omega_{\text{H I}} = 4.2^{+9.6}_{-3.5} \times 10^{-5}$  for DLAs and sub-DLAs respectively. The neutral gas density in DLAs at  $z \sim 0.6$  has been determined by previous surveys to be  $\Omega_{\text{H I}} = (9.7 \pm 3.6) \times 10^{-4}$  (Rao & Turnshek 2000; Rao, Turnshek & Nestor 2006).

The value determined here agrees within the errors with these previous determinations. The low- $z$  mass density of neutral gas from sub-DLA systems has not yet been thoroughly investigated. At  $z \sim 2.0$ , Péroux et al. (2005) find  $\Omega_{\text{H I}} = (1.9 \pm 1.3) \times 10^{-4}$ .

Due to the small number statistics, this sample is dominated by statistical errors. Upper and lower bounds on the gas density have been determined by using the upper and lower  $1\sigma$  limits on the number of systems,  $n^{\pm}$ , from Gehrels (1986) assuming Poisson statistics. We estimate the  $1\sigma$  range of  $\Sigma N(\text{H I})$  in Equation 4 as  $\Sigma N(\text{H I}) = n^{\pm} \langle N(\text{H I}) \rangle$  where  $\langle N(\text{H I}) \rangle$  is the mean *observed* column density in the sample.

## 6. SUMMARY AND DISCUSSION

In this work, we have reported on the first Damped Lyman- $\alpha$  systems observed with the Cosmic Origins Spectrograph. We summarize the results of this work as follows.

1) We have determined the redshift density and gas density of DLAs and sub-DLAs in this sample covering a total redshift path of  $\Delta z = 11.9$  at  $z < 0.34$ . We find  $dN/dz = 0.25_{-0.14}^{+0.24}$  and  $\Omega_{\text{H I}} = 1.4_{-0.7}^{+1.3} \times 10^{-3}$  for DLAs, and for sub-DLAs  $dN/dz = 0.08_{-0.06}^{+0.19}$  and  $\Omega_{\text{H I}} = 4.2_{-3.5}^{+9.6} \times 10^{-5}$ . The redshift density of DLAs determined here is several times higher than previous measurements of this value at  $z \sim 0.6$  of  $dN/dz = 0.079 \pm 0.019$  (Rao & Turnshek 2000; Rao, Turnshek & Nestor 2006). The large statistical errors of our sample make any differences unlikely to be statistically significant. No measure of  $dN/dz$  or  $\Omega_{\text{H I}}$  exists for sub-DLAs at  $z < 1.5$ , however the value determined here is lower than  $dN/dz = 0.34_{-0.19}^{+0.33}$  and  $\Omega_{\text{H I}} = (1.9 \pm 1.3) \times 10^{-4}$  seen at  $z \sim 2.0$  (Péroux et al. 2005). The neutral gas density in DLAs measured here is slightly higher than what has been found in previous surveys at  $z \sim 0.6$  which find  $\Omega_{\text{H I}} = (9.7 \pm 3.6) \times 10^{-4}$  (Rao, Turnshek & Nestor 2006), but the allowed range is fully consistent with the previous measurements. Based on 21 cm emission maps of galaxies in the nearby Universe, (Zwaan et al. 2005) find  $\Omega_{\text{H I}} = (3.5 \pm 0.8) \times 10^{-4}$ , which is well below the value determined here.

2) We have measured the abundances of several elements of one DLA in the sample and shown that the system has a sub-solar total abundance with  $[\text{S}/\text{H}] = -0.62 \pm 0.18$ . This metallicity is significantly higher than typical high redshift DLAs, which have average metallicities  $\langle [\text{Zn}/\text{H}] \rangle \sim -1.25$ . The kinematical structure of the DLA is remarkably simple. Only two components are needed to fit the profiles and the velocity width is well below that of the average DLA population with  $\Delta v_{90} = 52 \text{ km s}^{-1}$ . Remarkably, the kinematics are similar to those of the extremely metal poor DLAs from Pettini et al. (2008), even though the metallicity of this DLA is  $\sim 100$  times greater than the DLAs in that sample.

3) Followup imaging with WFC3 reveals several star forming and presumably gas rich galaxies within  $10''$  of the QSO, as well as a large spiral galaxy at small impact parameter to the bright QSO. At first glance, any of these candidates appear to be promising candidates

for the host galaxy of the DLA system. Followup spectroscopy of the galaxies reveal that none of them are at a similar redshift to the DLA. Spectra of an H II region in the spiral galaxy show strong narrow emission lines at the redshift of the QSO. This, combined with the close alignment of the nucleus and disk of the galaxy leads us to identify the spiral galaxy as the host of the QSO. The QSO host is luminous, with  $M_{F625W} = -24.4$  based on a decomposition of the WFC3 image with GALFIT. A small feature is seen  $\sim 0.7$  arcseconds from the center of the QSO nucleus after PSF subtraction, adding another host galaxy candidate of the DLA. Even with this supporting data, the origin of the DLA host galaxy remains enigmatic and exemplifies some of the difficulties of discovering the host galaxies of such systems.

4) Independent of the morphological properties of the DLA host galaxy, we conclude that the sightline likely passes through the warm neutral medium of the host as the metals are very mildly depleted with  $[\text{S}/\text{Fe}] = +0.24 \pm 0.22$ ,  $[\text{S}/\text{Ni}] = +0.35 \pm 0.22$  and  $[\text{S}/\text{Ti}] = +0.28 \pm 0.15$  and both C II\* and C I are not detected. The depletion levels and low cold gas content are characteristic of higher  $z$  DLA systems (Prochaska et al. 2002; Meiring et al. 2006; Noterdaeme et al. 2009). We find that the line of sight depletion factor  $F_* = -0.11 \pm 0.24$ , characteristic of sightlines through the halo of the Milky Way, reaffirming the conclusion that the sightline is passing through warm neutral gas.

In a forthcoming paper we will report on the metallicities and depletions in the other DLAs and sub-DLAs in this sample, as well as the  $N(\text{H I})$ -weighted mean metallicity at  $z < 0.34$ . Few observations of S or Zn, undepleted elements in the ISM and accurate metallicity indicators, exist at  $z < 0.5$  which spans  $\sim 40$  percent of the age of the universe. No observations of Zn or S in sub-DLA systems exist in this redshift range. At low redshifts, where there has been more time for the successive buildup of metals in the ISM of galaxies and the abundances of DLAs should be higher than at high redshift, it will be possible to see if DLAs show an increase in the  $[N/\alpha]$  ratio characteristic of secondary production of N. Our data show that over its lifetime, the Cosmic Origins Spectrograph will have the ability to measure the abundances and physical properties of QSO absorbers at  $z \sim 0$  with nearly the same precision as what can be done at  $z \sim 2$  with large ground based observatories.

## ACKNOWLEDGMENTS

Some of the data presented herein were obtained at the W.M. Keck Observatory, which is operated as a scientific partnership among the California Institute of Technology, the University of California and the National Aeronautics and Space Administration. The Observatory was made possible by the generous financial support of the W.M. Keck Foundation. The authors wish to extend special thanks to those of Hawaiian ancestry on whose sacred mountain we are privileged to be guests. Without their generous hospitality these observations would not have been possible. Financial support for this research was provided by NASA grants HST-GO-11598.03-A and

NNX08AJ44G. J.X.P. also acknowledges support from NSF grant (AST-0709235).

## REFERENCES

- Bahcall J.N., Kirhakos S., Saxe D.H., Schneider D.P., 1997, *ApJ*, 479, 642
- Becker R.H., White R.L., Helfand D.J., 1995, *ApJ*, 450, 559
- Blanton M.R., Hogg D.W., Bahcall N.A., Brinkman J., Britton M., Connolly A.J., Csabai I., Loveday J., et al., 2003, *ApJ*, 592, 819
- Borthakur S., Tripp T.M., Yun M.S., Momjian E., Meiring J.D., Bowen D.V., York D.G., 2010, *ApJ*, 713, 131
- Bowen D.V., Tripp T.M., Jenkins E.B., 2001, *AJ*, 121, 1456
- Bowen D.V., Jenkins E.B., Pettini M., Tripp T.M., 2005, *ApJ*, 635, 880
- Centurión M., Molaro P., Vladilo G., Péroux C., Levshakov S.A., D’Odorico V., 2003, *A&A*, 403, 55
- Elmegreen B.G., Parravano A., 1994, *ApJ*, 435, 121
- Fitzpatrick E. L., Spitzer, L., 1994, *ApJ*, 427, 232
- Froning C.S., Green J.C., *Ap&SS*, 320, 181
- Gehrels N., 1986, *ApJ*, 303, 336
- Ghavamian, P., et al. 2009, Preliminary Characterization of the Post-Launch Line Spread Function of COS, <http://www.stsci.edu/hst/cos/documents/isrs/>
- Goddard Q.E., Kennicutt R.C., Ryan-Weber E.V., 2010, *MNRAS*, 405, 2791
- Haardt F., Madau P., 1996, *ApJ*, 461, 20
- Henry R. B. C., Prochaska J.X., 2007, *PASP*, 119, 962
- Hamilton T.S., Casertano S., Turnshek D.A., 2002, *ApJ*, 576, 61
- Jenkins E.B., Tripp T.M., 2001, *ApJS*, 137, 297
- Jenkins E.B., Tripp T.M., 2006, *ApJ*, 637, 548
- Jenkins E.B., 2009, *ApJ*, 700, 1299
- Kennicutt R.C., 1998, *ApJ*, 498, 541
- Kulkarni V.P., Khare P., Som D., Péroux C., York D.G., Meiring J.D., Lauroesch J.T., 2010, *New Astronomy*, in press
- Liszt H., 2002, *A&A*, 389, 343
- Ledoux, C. Petitjean, P., Moller, P., Fynbo, J., Srianand R., 2006, *A&A*, 457, 71
- Lehner N., Wakker B.P., Savage B.D., 2004, *ApJ*, 615, 757
- Lodders, K., 2003, *ApJ*, 591, 1220
- Lupton R., Blanton M.R., Fekete G., Hogg D.W., O’Mullane W., Szalay A., Wherry N., 2004, *PASP*, 116,133
- Meiring J.D., Kulkarni V.P., Khare P., Bechtold J., York D.G., Cui J., Lauroesch J.T., Crofts A.P.S., Nakamura O., 2006, *MNRAS*, 370, 43
- Meiring J.D., Kulkarni V.P., Lauroesch J.T., Péroux C., Khare P., York D.G., 2009, *MNRAS*, 393, 1513
- Meiring J.D., Lauroesch J.T., Kulkarni V.P., Péroux C., Khare P., York D.G., 2009, *MNRAS*, 397, 2037
- Marigo P., 2001, *A&A*, 370, 194
- Noterdaeme P., Ledoux C., Petitjean P., Srianand R., 2009, *A&A*, 327, 336
- Noterdaeme P., Petitjean P., Ledoux C., Srianand R., 2009, *A&A*, 1087, 1098
- Noterdaeme P., Srianand R., Mohan V., 2010, *MNRAS*, 403, 906
- Peng C.Y., Ho L.C., Impey C.D., Rix H.W., 2010, *AJ*, 139, 2097
- Pettini M., Zych B.J., Steidel C.C., Chaffee F.H., 2008, *MNRAS*, 385, 2011
- Prochaska J. X., Wolfe A. M., 1997, *ApJ*, 487, 73
- Prochaska J.X., Wolfe A.M., 2002, *ApJ*, 566, 68
- Prochaska J.X., Gawiser E., Wolfe A.M., Castro S., Djorgovski S. G., 2003, *ApJ*, 595, L9
- Prochaska J.X., Howk J.C., O’Meara J.M., Tytler D., Wolfe A.M., Kirkman D., Lubin D., Suzuki N., 2002, *ApJ*, 571, 693
- Prochaska J.X., Herbert-Fort S., Wolfe A.M., 2005, *ApJ*, 635, 123
- Prochaska J.X., O’Meara J.M., Herbert-Fort S., Burles S., Prochter G.E., Bernstein R.A., 2006, *ApJL*, 648, 97
- Péroux C., Dessauges-Zavadsky M., D’Odorico S., Kim T.S., McMahon R., 2003, *MNRAS*, 345, 480
- Péroux C., McMahon R.G., Storrie-Lombardi L.J., Irwin M.J., 2003, *MNRAS*, 346, 1103
- Péroux C., Dessauges-Zavadsky M., D’Odorico S., Kim T.S., McMahon R.G., *MNRAS*, 363, 479
- Rao S.M., Turnshek D.A., 2000, *ApJ*, 130, 1
- Rao S.M., Turnshek D.A., Nestor D.B., 2006, *ApJ*, 636, 610
- Ribaudo J., Lehner N., Howk C.J., 2010, *ApJ*, submitted
- Savage B.D., Sembach K.R., 1996, *ARAA*, 34, 279
- Schaye J., 2004, *ApJ*, 609, 667
- Schlegel D.J., Finkbeiner D.P., Davis M., 1998, *ApJ*, 500, 525
- Sembach K.R., Savage B.D., 1996, *ApJ*, 457, 211
- Srianand R., Petitjean P., Ledoux C., Ferland G., Shaw G., 2005, *MNRAS*, 362, 549
- Storrie-Lombardi L.J., Wolfe A.M., 2000, *ApJ*, 543, 552
- Thom C., Werk J.E., Tumlinson J., Prochaska J.X., Meiring J.D., Tripp T.M., Sembach K.R., 2011, *ApJ*, submitted
- Toomre A., 1964, *ApJ*, 139, 1217
- Tremonti C.A., Heckman T.M., Kauffmann G., Brinchmann J., Charlot S., White S.D.M., Seibert M., Peng E.W., et al. 2004, *ApJ*, 613, 898
- Tripp T.M., Jenkins E.B., Bowen D.V., Prochaska J.X., Aracil B., Ganguly R., 2005, *ApJ*, 619, 714
- Tumlinson J.T., Werk J.K., Thom C.T., Meiring J.D., Prochaska J.X., Tripp T.M., Okrochkov M., Sembach K.R., 2011, submitted
- Van Zee L., Salzer J.J., Haynes M.P., O’Donoghue A.A., 1998, *ApJ*, 116, 2805
- Van Zee L., Haynes M.P., 2006, *ApJ*, 636, 214
- Vogt et al., 1994, *Proc. SPIE*, 2198, 362
- Morton D.C., 2003, *ApJS*, 149, 205
- Wakker B.P., 2006, *ApJ*, 163, 282
- Welty D. E., Lauroesch J.T., Blades J.C., Hobbs L.M., York, D.G., 1997, *ApJ*, 489, 672
- Wolfe A.M., Lanzetta K.M., Foltz C.B., Chaffe F., 1995, *ApJ*, 454, 698
- Wolfe A.M., Prochaska J.X., Gawiser E., 2003, *ApJ*, 593, 215
- Wolfe A.M., Gawiser E., Prochaska J.X., 2005, *Annu. Rev. Astron. Astrophys.*, 43, 861
- Wright E.L., 1991, *ApJ*, 381, 200
- York D.G., Adelman J., Anderson J.E., Jr., Anderson S.F., Annis J., Bahcall N.A., Bakken J. A., Barkhouser R., et al. 2000, *AJ*, 120, 1579
- Zwaan M. A., Meyer M.J., Staveley-Smith L., Webster R.L., 2005, *MNRAS*, 359, 30